Beyond the charge radius: The information content of the fourth radial moment

P.-G. Reinhard [1] W. Nazarewicz [2] and R. F. Garcia Ruiz[3,4]

[1]*Institut für Theoretische Physik, Universität Erlangen, D-91054 Erlangen, Germany*
[2]*Department of Physics and Astronomy and FRIB Laboratory, Michigan State University, East Lansing, Michigan 48824, USA*
[3]*Physics Department, CERN, CH-1211 Geneva 23, Switzerland*
[4]*Massachusetts Institute of Technology, Cambridge, Massachusetts 02139, USA*

Measurements of atomic transitions in different isotopes offer key information on the nuclear charge radius. The anticipated high-precision experimental techniques, augmented by atomic calculations, will soon enable extraction of the higher order radial moments of the charge density distribution. To assess the value of such measurements for nuclear structure research, we study the information content of the fourth radial moment $\langle r^4 \rangle$ by means of nuclear density functional theory and a multiple correlation analysis. We show that $\langle r^4 \rangle$ can be directly related to the surface thickness of nuclear density, a fundamental property of the atomic nucleus that is difficult to obtain for radioactive systems. Precise knowledge of these radial moments is essential to establish reliable constraints on the existence of new forces from precision isotope shift measurements.

Introduction. A precise knowledge of the electron-nucleus interaction in atoms can provide access to physical phenomena relevant to a wide range of energy scales. High-precision measurements of atomic transitions, for example, offer complementary information to our understanding of the atomic nucleus, the study of fundamental symmetries, and the search for new physics beyond the standard model of particle physics [1–4].

Varying the number of neutrons induces changes in the charge density distribution along the isotopic chain, causing tiny perturbations in the energies of their atomic electrons, known as isotope shifts. Measurements of the corresponding frequencies, typically of the order of MHz, allow changes in the root-mean-squared (rms) nuclear charge radii to be extracted [5,6]. Extending these measurements for isotopes away from stability is of marked and growing interest for low-energy nuclear physics, as the data on the nuclear size are essential for our understanding of the nuclear many-body problem [5,7–10]. In recent years, the interest in precision isotope shift measurements has increased significantly. Performing measurements across long isotope chains that are readily available at state-of-the-art radioactive ion beam facilities has the potential to constrain the existence of new forces and hypothetical particles with unprecedented sensitivity [2–4,11–14]. This has motivated the rapid progress of experimental techniques which are continuously pushing the frontiers of precision measurements. Quantum logic detection schemes have achieved sub-MHz precision [15], and recent developments such as spin squeezing [16] and quantum entanglement [17] are now able to reach sub-Hz precision. This level of precision offers sensitivity not only would allow us to explore new physics but would also provide access to nuclear observables that have so far been elusive, such as the higher order radial moment $\langle r^4 \rangle$ [18,19] and the nuclear dipole polarizability [13]. Precise knowledge of these nuclear properties will open up exciting opportunities in nuclear structure research and hence is essential to establish reliable constraints in the exploration of new physics [13,14]. In addition to the progress of high-precision experiments, the continued development of atomic and nuclear theory has played a crucial role in extracting nuclear structure and fundamental physics observables from measurements [18–20].

The isotope shift, $\Delta \nu_i$, between an isotope with mass, A, and an isotope A', can be expressed by a product of nuclear and atomic factors as

$$\Delta \nu_i^{AA'} = K_{\mathrm{MS},i} \frac{A - A'}{AA'} + \sum_k F_{i,k} \delta \langle r^{2k} \rangle^{AA'}, \quad (1)$$

where $\delta \langle r^{2k} \rangle^{AA'}$ is the difference between the nuclear radial moments of order $2k$. The atomic part is factorized in the constants $K_{\mathrm{MS},i}$ and F_i, referred to as the mass shift and the field shift, respectively. Assuming a negligible contribution from $k > 1$ moments, isotope shifts from different atomic transition i and j, $\Delta \nu_i^{AA'}$ versus $\Delta \nu_j^{AA'}$, should follow a linear relation known as the King plot [21]. The nonlinearity of the King plot can be due to the contribution from $k > 1$ moments. It can also indicate the presence of new phenomena [2–4,11–13]. Therefore, the estimation of the effect higher order terms is important to provide bounds on physics beyond the standard model. As discussed in Refs. [18,19], taking advantage of the improved experimental precision and atomic calculations with

well-controlled uncertainty quantification for atomic states will enable us to extract highly accurate atomic line field shifts and higher order radial moments. To assess the impact of the anticipated data on our understanding of atomic nuclei, in this Rapid Communication, we employ density functional theory to study the $k = 2$ moment $\langle r^4 \rangle$ of nuclear charge distribution.

Nuclear charge distribution characteristics. The gross features of the nuclear charge distribution $\rho(\boldsymbol{r})$ and its charge form factor $F(\boldsymbol{q})$ can be described by form parameters: radial moments

$$r_n \equiv \sqrt[n]{\langle r^n \rangle} = \left(\frac{\int d^3 r\, r^n\, \rho(\boldsymbol{r})}{\int d^3 r\, \rho(\boldsymbol{r})} \right)^{1/n}, \qquad (2)$$

diffraction radius R, and surface thickness σ. The latter characterizes the density diffuseness around the nuclear surface. The rms charge radius is given by the second moment r_2. The diffraction radius is determined from the first zero of the form factor $F(q)$ (the diffraction minimum). It represents a box-equivalent radius. The surface thickness is determined from the height of the first maximum of $F(q)$. The relations between spatial geometrical parameters and the form factor are provided by the Helm model [22], which represents the nuclear density profile by a folding of a box distributions (having radius R) with a Gaussian of width σ. For details, see Refs. [23–26] and the Supplemental Material [27]. Within the Helm model, r_2 can be expressed in terms of R, and σ: $r_2^{(H)} = \sqrt{\frac{3}{5}R^2 + 3\sigma^2}$. In practice, this relation is not exactly fulfilled and the deviation characterizes the halo of the charge distribution [28–30]:

$$h = r_2 - r_2^{(H)}. \qquad (3)$$

In practice, the halo is a small positive quantity [28]. Diffused charge distributions associated with loosely bound protons in proton-rich isotopes produce appreciable values of h. To give an idea about the typical values and trends, we show in Fig. 1 the charge density form parameters for the chain of Sn isotopes calculated with two nuclear energy density functionals: the Skyrme parametrization SV-min [31] and the Fayans functional Fy(Δr,HFB) [10,27,32]. (For the treatment of pairing in natural orbital representation in Fy(Δr,HFB) see Refs. [33–35].) Both functionals have been optimized with respect to the pool of empirical data from [31], with some additional charge radii data used in the optimization of Fy(Δr,HFB). The fits allow us also to deduce the statistical uncertainties on the predicted observables by standard linear regression methods [36]. The uncertainties are consistent with the adopted errors for the observables, which are ± 0.04 fm for R and σ and ± 0.02 fm for r_2. These errors do not contain the experimental uncertainties but reflect the capability of the model to reproduce observables. A measurement is expected to provide new information if the experimental uncertainty is safely below the model error. The values of the form parameters show the expected trends [28]. Namely, the proton radii shrink systematically with increasing neutron number because of the increasing proton binding. The pronounced kink at the $N = 82$ shell closure seen in all form parameters is due to reduced neutron pairing [9]. The two density functionals used deliver similar results in the domain of
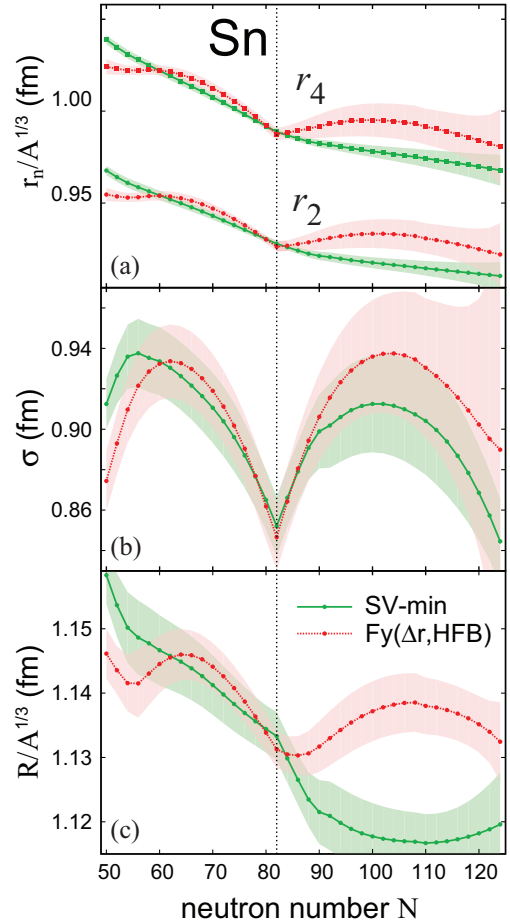

FIG. 1. Form parameters along the Sn chain ($Z = 50$) computed with energy density functionals SV-min and Fy(Δr) together with their statistical uncertainties. Shown are radial moments r_2 and r_4 (a), surface thickness σ (b), and diffraction radii R (c). To better visualize the local trends, radial moments and diffraction radii are scaled by $A^{1/3}$. The magic neutron number $N = 82$ is marked.

well-bound nuclei while developing slight differences at exotic proton-rich nuclei close to $N = 50$ and neutron-rich nuclei with $N > 82$. This is entirely anticipated: Form parameters of stable nuclei, being part of the optimization data pool, are bound to be well reproduced. The differences between SV-min and Fy(Δr,HFB) in neutron-rich isotopes are almost exclusively generated by the gradient-pairing term of the Fayans functional. At the neutron-rich side, the difference for the diffraction radii R can amount up to about 0.1 fm, clearly above the error bars.

Statistical analysis. The information content of r_4 is evaluated using standard statistical correlation analysis as in Refs. [9,37]. The question we ask is to what extent r_4 is already determined by the other form parameters and, vice versa, to what extent information on r_4 improves our knowledge of R and σ. The answer can be quantified in terms of statistical correlations. Those between two observables A and B are described by the coefficient of determination CoD(A, B) deduced from the covariance measure. Furthermore, we inspect multiple correlation coefficients MCC($A_1, ..., A_n; B$),
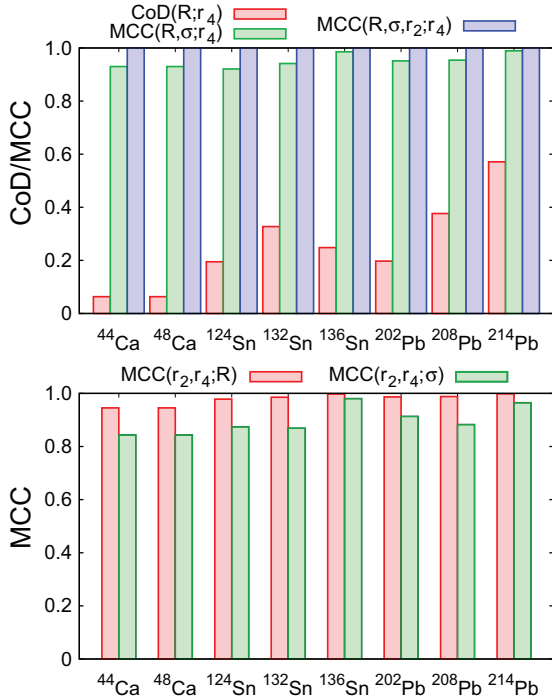
FIG. 2. Top: CoD and MCC coefficients between the standard form parameters and r_4 for a selection of spherical nuclei. Bottom: information content of r_2 and r_4 in terms of MCCs between r and r_4 with the form parameters R or σ.

FIG. 3. Helm-model SV-min predictions (4)–(7) for σ (top) and R (bottom) for the chain of Sn isotopes. The values of σ and R extracted from the charge density form factor are also shown together with their uncertainties.

which characterize the correlations between a group of observables $A_1, ..., A_n$ with B [38]. The MCC is reduced to the CoD if $n = 1$. The CoDs and MCCs range from 0 to 1, where 0 implies that the observable B is uncorrelated with the group of observables A_i and the value of 1 means full correlation.

The results of our correlation analysis are shown in Fig. 2. The upper panel explores the prediction of r_4 for known R, σ, and r_2 for a set of spherical nuclei, which have very small halo. The diffraction radius alone has little predictive value for r_4. This is not surprising as R carries no information on surface diffuseness, which strongly impacts the fourth radial moment. The combination of R and σ provides a very good 95% estimate of r_4. Finally, the group of R and σ, and r_2 (or h) manages to determine r_4 fully.

The lower panel of Fig. 2 explores whether a simultaneous measurement of r_2 and r_4 can determine R or σ. The MCCs show that the diffraction radius is indeed very well determined by r_2 and r_4, especially for heavy nuclei. The surface thickness is also well predicted, although not as perfectly as R, typically at a 90% level.

Helm model analysis. Statistical analysis, although well defined and extremely useful, remains largely a black box. To gain more physics insights, we study interrelations between the form parameters as mediated by the Helm model, which is commonly used to inform nuclear energy density functionals about experimental charge form factor. We checked some alternative models with more realistic exponential asymptotics [25], and after finding no significant differences in the context of our work, we decided to stick to the Helm model as the simplest one. Given r_2 and r_4, we deduce closed approximate
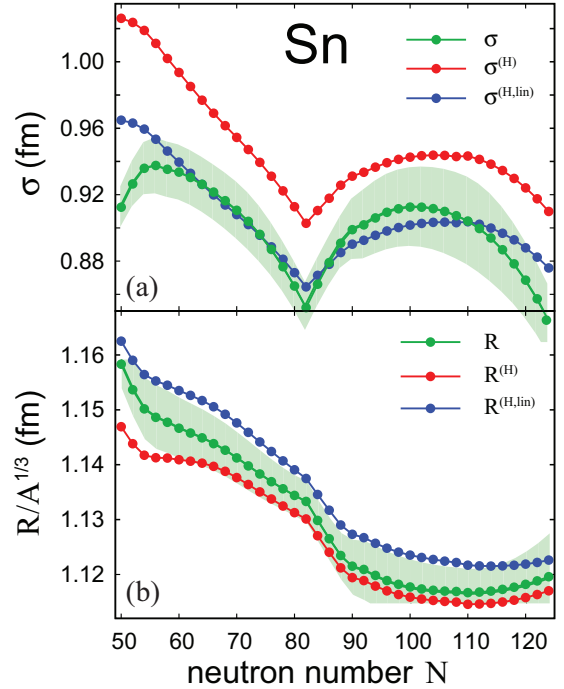
expression for σ and R, again denoted by an upper index (H) to distinguish them from the exact values; see Ref. [27] for details. For more compact expressions, we introduce the rescaled geometric radii as $R_n^{(g)} = \sqrt[n]{\frac{n+3}{3} r_n^n}$ [28].

In terms of $R_2^{(g)}$ and $R_4^{(g)}$ the Helm-model values of diffraction radius and surface thickness are [27]

$$R^{(H)} = \sqrt[4]{\frac{7}{2}R_2^{(g)4} - \frac{5}{2}R_4^{(g)4}}, \tag{4}$$

$$\sigma^{(H)} = \sqrt{\frac{1}{5}R_2^{(g)2}\left(1 - \sqrt{1 - \frac{5}{2}\frac{R_4^{(g)4} - R_2^{(g)4}}{R_2^{(g)4}}}\right)}. \tag{5}$$

Another set of useful relations can be obtained by noticing that σ^2/R^2 is a small parameter, which is around 0.02–0.03 (see Fig. 1). By linearizing the above relations with respect to σ^2/R^2, one obtains the following approximate relations:

$$R^{(H),lin} \approx R_2^{(g)} + \frac{7}{2}\left(R_4^{(g)} - R_2^{(g)}\right), \tag{6}$$

$$\sigma^{(H),lin} \approx \sqrt{\left(R_4^{(g)} - R_2^{(g)}\right)R_2^{(g)}}, \tag{7}$$

$$\frac{R_4^{(g)} - R_2^{(g)}}{R_2^{(g)}} \approx \left(\frac{\sigma^{(H),lin}}{R^{(H),lin}}\right)^2. \tag{8}$$

Figure 3 compares the Helm model values of R and σ given by Eqs. (4)–(7) to the exact values directly obtained form the charge density form factor in the Sn isotopic chain (for
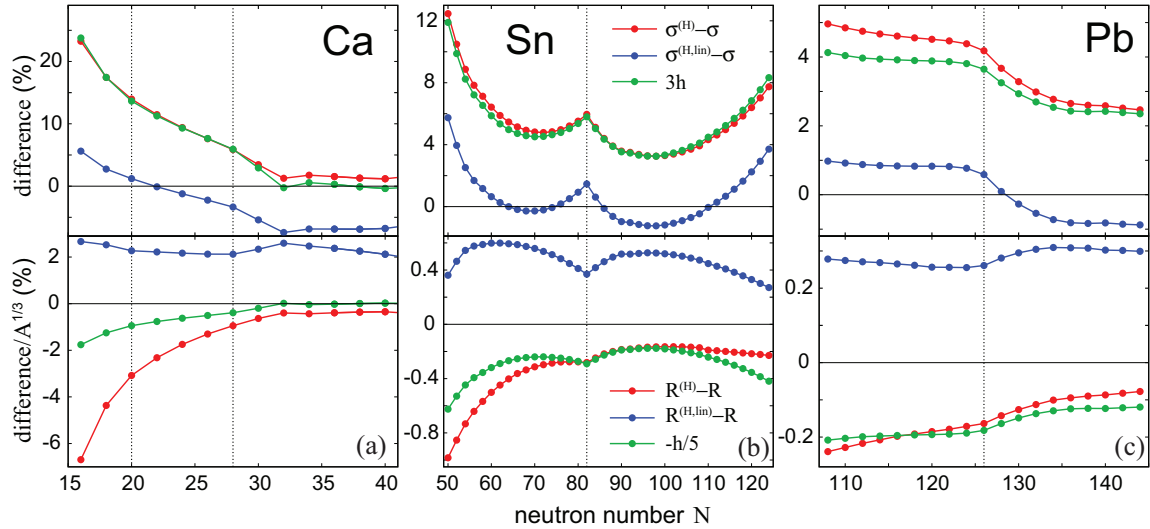
FIG. 4. Relative difference of Helm-model predictions (4)–(7) from the form factor values of R (lower) and σ (upper) for the isotopic chains of Ca (a), Sn (b), and Pb (c) computed with SV-min.

Ca and Pb chains, see Ref. [27]). The predictions based on r_2 and r_4 are fairly accurate. Indeed, for both R and σ, the deviations of the Helm estimates from the form factor values are close to the computed uncertainties. Particularly good is the agreement for R as the deviation between $R^{(H)}$ and R, around 0.02 fm is smaller than the adopted error of diffraction radii (0.04 fm). Interestingly, the linearized $\sigma^{(H),lin}$ performs exceptionally well except for the most proton-rich isotopes, in which the appreciable halo feature appears.

Figure 4 shows the relative differences (in %) between form parameters R and σ and the Helm-model predictions for three different magic chains: Ca, Sn, and Pb [see Ref. [27] for the absolute differences in fm, and for additional information on $(\sigma/R)^2$]. It is seen that the quality of the Helm-model predictions improves significantly with increasing system size (see Ref. [39]). The density distributions of Ca isotopes are strongly impacted by surface effects and thus harder to describe by the simple Helm parametrization, while the Pb isotopes are volume dominated; hence, they are well approximated by the Helm model. But the general features observed before for the Sn chain remain: R is better predicted than σ, and the linearized prediction for σ performs unexpectedly well for all isotopic chains (though at different levels of overall quality).

Altogether, we see that the Helm-model analysis nicely corroborates the findings from statistical analysis. Figure 4 contains one more piece of information: It compares the differences with multiples of the halo parameter (3). It is interesting to see that the differences $R^{(H)} - R$ and $\sigma^{(H)} - \sigma$ are proportional to h. This observation is fairly consistent within the model. Zero halo means that the exact distribution is described fully by the Helm model. In this case, the differences would be zero. A mismatch leads to a finite halo and the same mismatch propagates to the predictions. This suggests a way to develop model-corrected predictions for R and σ from r_n measurements. For a given isotopic chain, the halos follow regular trends which can be tracked in

density-functional calculations. Namely, one can correct the Helm-model predictions by predicted halo values to obtain the form parameters R and σ in exotic nuclei from r_n measurements with well-defined uncertainties that are well below those of the Helm model.

Conclusions. In this study, we assessed the impact of precise experimental determination of $\langle r^4 \rangle$ on nuclear structure research. By means of statistical correlation analysis, we demonstrated that the diffraction radius R and surface thickness σ are well determined by $\langle r^2 \rangle$ and $\langle r^4 \rangle$, especially for heavy nuclei. Using the Helm model for the charge density, we could develop simple and robust relations for predicting R and σ from given $\langle r^2 \rangle$ and $\langle r^4 \rangle$. A higher predictive power is obtained when using $\langle r^2 \rangle$ and $\langle r^4 \rangle$ as input to fits of self-consistent model and retrieving R and σ from them. This result was obtained by studying a broad selection of semimagic spherical nuclei. We expect that our conclusions apply for moderately deformed nuclei because it is a spherically averaged (monopole) charge density that is used in the analysis of the isotope shifts. The situation is less clear, however, for exotic topologies of charge density as, e.g., in nuclei with an appreciable spherical depression. In such cases, the Helm model needs to be modified to account for new effects [37,40].

It is to be noted that for the nuclei for which the charge density/form factor is experimentally known in the large range of r, the values of r_4 are well constrained by electron scattering data. In this context, we note that the values of R and σ, and often also r_2, are determined from the charge form factor at low momentum transfer q, typically $q < 6/A^{1/3}$ fm^{-1} [23].

Our findings are well aligned with the recent experimental progress [1,5,15–18,41–43]. We hope these results will provide a strong motivation for the next generation of precision experiments at radioactive beam facilities worldwide. Experimental determination of $\langle r^4 \rangle$ would be extremely valuable for nuclei where the form factor data are not available. Since electron scattering experiments on unstable nuclei are highly

demanding, if not impossible, precise measurements of atomic transitions would offer an alternative path to surface properties of unstable nuclei. Finally, as shown in Fig. 1, information on $\langle r^4 \rangle$ would be very useful for better constraining current energy density functionals.

[1] M. S. Safronova, D. Budker, D. DeMille, D. F. J. Kimball, A. Derevianko, and C. W. Clark, Rev. Mod. Phys. **90**, 025008 (2018).

[2] J. C. Berengut, D. Budker, C. Delaunay, V. V. Flambaum, C. Frugiuele, E. Fuchs, C. Grojean, R. Harnik, R. Ozeri, G. Perez, and Y. Soreq, Phys. Rev. Lett. **120**, 091801 (2018).

[3] Y. V. Stadnik, Phys. Rev. Lett. **120**, 223202 (2018).

[4] C. Delaunay, C. Frugiuele, E. Fuchs, and Y. Soreq, Phys. Rev. D **96**, 115002 (2017).

[5] R. F. Garcia Ruiz, M. L. Bissell, K. Blaum, A. Ekström, N. Frömmgen, G. Hagen, M. Hammen, K. Hebeler, J. D. Holt, G. R. Jansen *et al.*, Nat. Phys. **12**, 594 (2016).

[6] P. Campbell, I. Moore, and M. Pearson, Prog. Part. Nucl. Phys. **86**, 127 (2016).

[7] M. Hammen, W. Nörtershäuser, D. L. Balabanski, M. L. Bissell, K. Blaum, I. Budincevic, B. Cheal, K. T. Flanagan, N. Frömmgen, G. Georgiev, C. Geppert, M. Kowalska, K. Kreim, A. Krieger, W. Nazarewicz, R. Neugart, G. Neyens, J. Papuga, P.-G. Reinhard, M. M. Rajabali, S. Schmidt, and D. T. Yordanov, Phys. Rev. Lett. **121**, 102501 (2018).

[8] B. A. Marsh, T. Day Goodacre, S. Sels, Y. Tsunoda, B. Andel, A. N. Andreyev, N. A. Althubiti, D. Atanasov, A. E. Barzakh, J. Billowes *et al.*, Nat. Phys. **14**, 1163 (2018).

[9] C. Gorges, L. V. Rodríguez, D. L. Balabanski, M. L. Bissell, K. Blaum, B. Cheal, R. F. Garcia Ruiz, G. Georgiev, W. Gins, H. Heylen, A. Kanellakopoulos, S. Kaufmann, M. Kowalska, V. Lagaki, S. Lechner, B. Maaß, S. Malbrunot-Ettenauer, W. Nazarewicz, R. Neugart, G. Neyens, W. Nörtershäuser, P.-G. Reinhard, S. Sailer, R. Sánchez, S. Schmidt, L. Wehner, C. Wraith, L. Xie, Z. Y. Xu, X. F. Yang, and D. T. Yordanov, Phys. Rev. Lett. **122**, 192502 (2019).

[10] A. J. Miller, K. Minamisono, A. Klose, D. Garand, C. Kujawa, J. D. Lantis, Y. Liu, B. Maaß, P. F. Mantica, W. Nazarewicz *et al.*, Nat. Phys. **15**, 432 (2019).

[11] C. Delaunay, R. Ozeri, G. Perez, and Y. Soreq, Phys. Rev. D **96**, 093001 (2017).

[12] C. Frugiuele, E. Fuchs, G. Perez, and M. Schlaffer, Phys. Rev. D **96**, 015011 (2017).

[13] V. V. Flambaum, A. J. Geddes, and A. V. Viatkina, Phys. Rev. A **97**, 032510 (2018).

[14] K. Mikami, M. Tanaka, and Y. Yamamoto, Eur. Phys. J. C **77**, 896 (2017).

[15] F. Gebert, Y. Wan, F. Wolf, C. N. Angstmann, J. C. Berengut, and P. O. Schmidt, Phys. Rev. Lett. **115**, 053003 (2015).

[16] B. Braverman, A. Kawasaki, E. Pedrozo-Peñafiel, S. Colombo, C. Shu, Z. Li, E. Mendez, M. Yamoah, L. Salvi, D. Akamatsu, Y. Xiao, and V. Vuletić, Phys. Rev. Lett. **122**, 223203 (2019).

[17] T. Manovitz, R. Shaniv, Y. Shapira, R. Ozeri, and N. Akerman, Phys. Rev. Lett. **123**, 203001 (2019).

[18] A. Papoulia, B. G. Carlsson, and J. Ekman, Phys. Rev. A **94**, 042502 (2016).

[19] J. Ekman, P. Jönsson, M. Godefroid, C. Nazé, G. Gaigalas, and J. Bieroń, Comput. Phys. Commun. **235**, 433 (2019).

[20] B. K. Sahoo, A. R. Vernon, R. F. Garcia Ruiz, C. L. Binnersley, J. Billowes, M. L. Bissell, T. E. Cocolios, G. J. Farooq-Smith, K. T. Flanagan, W. Gins *et al.*, New J. Phys. **22**, 012001 (2020).

[21] W. King, *Isotope Shifts in Atomic Spectra* (Springer Science & Business Media, Berlin, 2013), Vol. 11, p. 210.

[22] R. H. Helm, Phys. Rev. **104**, 1466 (1956).

[23] J. Friedrich and N. Vögler, Nucl. Phys. A **373**, 192 (1982).

[24] J. Friedrich and P.-G. Reinhard, Phys. Rev. C **33**, 335 (1986).

[25] D. Andrae, Phys. Rep. **336**, 413 (2000).

[26] M. Bender, P.-H. Heenen, and P.-G. Reinhard, Rev. Mod. Phys. **75**, 121 (2003).

[27] See Supplemental Material at http://link.aps.org/supplemental/10.1103/PhysRevC.101.021301 for details on the form parameters of the nuclear charge distribution; supplemental figures illustrating the differences between Helm-model predictions and form parameters; and the Fy(Δr,HFB) parameters.

[28] S. Mizutori, J. Dobaczewski, G. A. Lalazissis, W. Nazarewicz, and P.-G. Reinhard, Phys. Rev. C **61**, 044326 (2000).

[29] P. Sarriguren, M. K. Gaidarov, E. M. deGuerra, and A. N. Antonov, Phys. Rev. C **76**, 044322 (2007).

[30] N. Schunck and J. L. Egido, Phys. Rev. C **78**, 064305 (2008).

[31] P. Klüpfel, P.-G. Reinhard, T. J. Bürvenich, and J. A. Maruhn, Phys. Rev. C **79**, 034310 (2009).

[32] P.-G. Reinhard and W. Nazarewicz, Phys. Rev. C **95**, 064328 (2017).

[33] P.-G. Reinhard, M. Bender, K. Rutz, and J. Maruhn, Z. Phys. A **358**, 277 (1997).

[34] S. J. Krieger, P. Bonche, H. Flocard, P. Quentin, and M. S. Weiss, Nucl. Phys. A **517**, 275 (1990).

[35] J. Erler, P. Klüpfel, and P.-G. Reinhard, Eur. Phys. J. A **37**, 81 (2008).

[36] J. Dobaczewski, W. Nazarewicz, and P.-G. Reinhard, J. Phys. G **41**, 074001 (2014).

[37] B. Schuetrumpf, W. Nazarewicz, and P.-G. Reinhard, Phys. Rev. C **96**, 024306 (2017).

[38] P. D. Allison, *Multiple Regression: A Primer* (Sage, Thousand Oaks, CA, 1998).

[39] P.-G. Reinhard, M. Bender, W. Nazarewicz, and T. Vertse, Phys. Rev. C **73**, 014309 (2006).

[40] J. Friedrich, N. Voegler, and P.-G. Reinhard, Nucl. Phys. A **459**, 10 (1986).

[41] M. G. Kozlov, M. S. Safronova, J. R. Crespo López-Urrutia, and P. O. Schmidt, Rev. Mod. Phys. **90**, 045005 (2018).

[42] C. A. Holliman, M. Fan, and A. M. Jayich, Phys. Rev. A **100**, 062512 (2019).

[43] M. Fan, C. A. Holliman, A. L. Wang, and A. M. Jayich, Phys. Rev. Lett. **122**, 223001 (2019).